19

Analysis of the influence of quantum effects on photothermal properties of layered nanoparticles using the discrete sources method

© Yu.A. Eremin, V.V. Lopushenko

Moscow State University, Moscow, Russia

e-mail: lopushnk@cs.msu.ru

Received November 17, 2025
Revised December 29, 2025
Accepted December 30, 2025

The discrete sources method is used to study the influence of quantum effects arising in the gold and silver cores of layered nanoparticles with a dense dielectric coating. This coating is designed to prevent particle clustering without reducing the energy absorbed by the particle. The study found that the absorption cross section of layered particles with a silver core is four times larger than that of particles with a gold core. It was also determined that the dielectric coating does not reduce the absorbed energy compared to homogeneous metal nanoparticles. It was shown that varying the elongation of the core allows the absorption cross section maximum to be shifted toward the transparency region of biological tissue, while varying the equivolume diameter of the core has virtually no effect on the position of the absorption cross section maximum in the wavelength range. The influence of quantum effects is limited to a shift of the absorption cross section maximum toward shorter wavelengths by 15 nm and a slight decrease in its magnitude.

Keywords: layered nanoparticles, gold and silver cores, quantum effects, mesoscopic boundary conditions, Feibelman parameters, discrete sources method.

DOI: 10.61011/EOS.2026.02.63473.8789-25

Introduction

Plasmonic nanoparticles (NPs) are used in numerous applications: gene engineering, biosensing, cancer therapy, internal organ imaging, and drug delivery [1]. In particular, cancer treatment is based on plasmonic photothermal therapy (PTT) using gold and silver NPs, which absorb electromagnetic energy and convert it into heat [2]. Most NPs developed for PTT intensively absorb radiation in the first near-infrared (IR) range ($\sim 650-950$ nm), where light penetrates living tissue better and non-targeted heating of healthy tissue surrounding the pathological mass is reduced [3].

NP size is an important factor that affects cellular absorption and intracellular distribution. NPs smaller than 10 nm may easily penetrate the cellular membranes providing for direct contact with the nuclear DNA and proteins. The studies have shown that small NPs are better absorbed by cells and penetrate a tumor more easily compared to the large ones [4]. Even though spherical NPs are more common, particles of anisotropic shape, such as rods, triangles and stars, are widely used in cancer diagnostics and treatment. Golden nanorods, for example, demonstrate a noticeable absorption in the near IR range, which makes it possible to conduct PTT of tumours located deeply in the tissues with their help [5]. Silver NPs also have useful optical properties, including higher values of absorption cross section than in the golden particles. Therefore, silver may provide for more effective conversion of light to heat compared to gold [6,7].

To protect organs against unwanted exposure to metals, the NP surface is functionalized by application of biocompatible polymer coatings, which guarantee stability of NPs, not decreasing their therapeutic efficacy at the same time. Functionalization of the NP surface is critical, since it causes reduction in the surface energy, acting as a barrier preventing aggregation of NPs into clusters and providing for their disperse distribution in the organs [8].

The ratio of the share of absorbed light converted to heat to the total absorbed energy determined by the NP absorption cross section is called the photothermal conversion efficacy. The comparative analysis of various geometries of plasmon NPs demonstrated that the photothermal conversion efficacy of nanorods is approximately twice higher than in nanoshells and nanostars, with the identical absorption cross section [3].

Miniaturization of NP dimensions is a current trend in improvement of PTT facilities. For example, it was found that the decreased golden NPs (30×7 nm) are better absorbed by tissue cells and have lower toxicity than standard ones (56×14 nm) [4]. However, quantum effects (QE) arise with such small dimensions, and affect the photothermal properties of plasmonic NPs in a certain way. The presence of such QEs as spatial nonlocality, displacement of the electron cloud relative to the NP surface, and Landau damping can significantly change both the position and amplitude of the plasmon resonance (PR), which acts as a key factor ensuring maximum energy absorption [9,10].

The aim of this work is to evaluate the influence of QEs arising in nanoscale cores of noble metals on the

absorption cross section in the diffraction problem on metal bodies with a dielectric coating. To analyze the influence of QEs on the absorbed energy level of layered NPs with a plasmonic core, we use a modification of the discrete sources method [11]. The QEs in the NP core are taken into account using mesoscopic boundary conditions with Feibelman parameters, the so-called surface response functions [12,13].

Boundary scattering problem

Let us consider the excitation with the linearly polarized plane electromagnetic wave of P-polarization of $\{\mathbf{E}_0, \mathbf{H}_0\}$ layered particle with a metal core (area D_i), coated with a layer of a transparent dielectric (area D_s). Let us consider that the particle has axial symmetry relative to the axis OZ. Let us designate the external unlimited area that surrounds a particle as D_e. We assume the surfaces of the metal core ∂D_i and dielectric layer ∂D_s to be rather smooth ($\partial D_{i,s} \in C^{(2,\tau)}$). All media are assumed to be non-magnetic, and the time dependence of the electromagnetic field has the following appearance $\exp(j\omega t)$.

Let us formulate the boundary problem of scattering for a layered NP with a dielectric coating. It includes the following equations and conditions.

1. A system of Maxwell's equations in the parameter constancy areas

$$\nabla \times \mathbf{H}_\alpha = jk\varepsilon_\alpha \mathbf{E}_\alpha, \ \nabla \times \mathbf{E}_\alpha = -jk\mathbf{H}_\alpha \text{ in } D_\alpha, \ \alpha = i, s, e. \tag{1}$$

2. Mesoscopic conditions for field coupling on the metal core surface

$$n_i \times (\mathbf{E}_i(P) - \mathbf{E}_s(P)) = -d_\perp \mathbf{n}_i \times \nabla \{\mathbf{n}_i \cdot (\mathbf{E}_i(P) - \mathbf{E}_s(P))\},$$

$$\mathbf{n}_i(\mathbf{H}_i(P) - \mathbf{H}_s(P)) = 0, \quad P \in \partial D_i. \tag{2}$$

3. Classic conditions of coupling on the external surface of the dielectric layer

$$\mathbf{n}_s \times (\mathbf{E}_s(Q) - \mathbf{E}_e(Q)) = \mathbf{n}_s \times \mathbf{E}_0(Q),$$

$$\mathbf{n}_s \times (\mathbf{H}_s(Q) - \mathbf{H}_e(Q)) = \mathbf{n}_s \times \mathbf{H}_0(Q), \quad Q \in \partial D_s. \tag{3}$$

4. Silver-Muller [14] radiation conditions at infinity

$$\lim_{r\to\infty} r \cdot \left(\sqrt{\varepsilon_e}\mathbf{E}_e(M) \times \frac{\mathbf{r}}{r} - \mathbf{H}_e(M)\right) = 0, \ r = |M|, M \in D_e. \tag{4}$$

Here $\{\mathbf{E}_e, \mathbf{H}_e\}$ — scattered field beyond a layered particle, $\{\mathbf{E}_i, \mathbf{H}_i\}$ — full field inside the core, $\{\mathbf{E}_s, \mathbf{H}_s\}$ — full field inside the shell, $\varepsilon_{e,s,i}$ — dielectric permittivity values of media in the corresponding areas, besides $\mathrm{Im}\varepsilon_{e,s} = 0$, $\mathrm{Im}\varepsilon_i \geq 0$, $\mathbf{n}_{i,s}$ — single external normal lines to the surfaces of interfaces with various characteristics $\partial D_{i,s}$, $k = \omega/c$.

The complex Feibelman parameter $d_\perp(\omega)$ is determined through the density of surface charges induced by the external field on the metal-dielectric interface. Its real part corresponds to the center of mass of the electron cloud of surface charges, the imaginary part describes the Landau damping. For the core of noble metals the real part of Feibelman parameter is $\mathrm{Re}d_\perp(\omega) \leq 0$ [12], which means „impression" of the electron cloud into the core.

Let us assume that the boundary problem (1)–(4) has the only solution.

Discrete sources method

To solve the set boundary problem, we will use the discrete sources method (DSM) [11]. DSM — is a numerically analytical, surface-oriented method in which the field representation is constructed as a sum of multipole fields located on the symmetry axis inside the layered particle. This approach automatically satisfies the system of Maxwell's equations (1) in the respective areas and the Silver-Müller radiation conditions (4) at infinity. The unknown coefficients (amplitudes) of discrete sources (DS) are determined from the mesoscopic coupling conditions (2) on the core surface and the standard coupling conditions (3) on the outer shell surface. It is important to emphasize that DSM is particularly effective in scattering problems with mesoscopic boundary conditions, since the fields generated by DS near the core surface are analytic functions [13]. This allows analytical computation of derivatives of any order on the core surface, which is necessary for satisfying the mesoscopic boundary conditions (2).

As external excitation, we will consider P-polarized wave spreading obliquely in respect to axis OZ. In this particular case the PR reaches its maximum value [13]. Let us assume that vector $\mathbf{E}_0$ is in the incidence plane XZ, and the angle between the wave vector and the rotation axis is $\pi - \theta_0$. In this case the external excitation field becomes

$$\mathbf{E}_0 = (\mathbf{e}_x \cos\theta_0 + \mathbf{e}_z \sin\theta_0)\chi(x, z),$$

$$\mathbf{H}_0 = -\sqrt{\varepsilon_e}\mathbf{e}_y \chi(x, z), \tag{5}$$

where $\chi(x, z) = \exp\{-jk_e(x \sin\theta_0 - z\cos\theta_0)\}$, $k_e = k\sqrt{\varepsilon_e}$, $(\mathbf{e}_x, \mathbf{e}_y, \mathbf{e}_z)$ — Cartesian basis.

To account for the axial symmetry of the scatterer, it is necessary to expand the field of the scalar plane wave $\chi(x, z)$ in (5) into a Fourier series of the form

$$\exp\{-jk_e x \sin\theta_0\} = \sum_{m=0}^{\infty} (2 - \delta_{0m})(-j)^m \times j_m(k_e\rho \sin\theta_0)\cos(m\varphi). \tag{6}$$

Here δ_{0m} — Kronecker symbol, j_m — cylindrical Bessel function, ρ, φ — cylindrical coordinates. Substituting (6) to (5) and changing from the Cartesian system to the cylindrical one, we obtain that the dependence of the field components on the azimuthal angle φ will be determined by functions $\cos[(m+1)\varphi]$ and $\sin[(m+1)\varphi]$.

We will build the fields in the areas $D_{i,s,e}$ on the basis of vector potentials, which in the cylindrical system of

coordinates may be recorded as follows [13]:

$$\mathbf{A}_{mn}^{1,\alpha} = Y_m^\alpha(\xi, z_n^\alpha)\{\mathbf{e}_\rho \cos[(m+1)\varphi] - \mathbf{e}_\varphi \sin[(m+1)\varphi]\}, \alpha = i, s, e,$$

$$\mathbf{A}_{mn}^{2,\alpha} = Y_m^\alpha(\xi, z_n^\alpha)\{\mathbf{e}_\varphi \sin[(m+1)\varphi] + \mathbf{e}_\varphi \cos[(m+1)\varphi]\},$$

$$\mathbf{A}_n^{3,\alpha} = Y_0^\alpha(\xi, z_n^\alpha)\mathbf{e}_z, \quad (7)$$

where the corresponding functions $Y_m^\alpha(\xi, z_n^\alpha)$ have the form

$$Y_m^e(\xi, z_n^e) = h_m^{(2)}(k_e R_{z_n^e})\left(\frac{\rho}{R_{z_n^e}}\right)^m,$$

$$Y_m^i(\xi, z_n^i) = j_m(k_i R_{z_n^i})\left(\frac{\rho}{R_{z_n^i}}\right)^m,$$

$$Y_m^{s\pm}(\xi, z_n^s) = h_m^{(2,1)}(k_s R_{z_n^s})\left(\frac{\rho}{R_{z_n^s}}\right)^m,$$

$h_m^{(1,2)}$ — spherical Hankel function, in $D_e h_m^{(2)}$ meets the radiation conditions, j_m — spherical Bessel functions, which are used for field representation inside the core, $k_{i,s,e} = k\sqrt{\varepsilon_{i,s,e}}$, $\xi = (\rho, z)$, $\rho^2 = x^2 + y^2$, $R_{z_n}^2 = \rho^2 + (z - z_n)^2$, $\{z_n^\alpha\}_{n=1}^{N_\alpha^m}$ — coordinates of DSs distributed along the rotation axis OZ, the number of which may vary depending on the number $m = \overline{1, M}$ of Fourier harmonic by φ.

Then the representations for fields $\{\mathbf{E}_\alpha, \mathbf{H}_\alpha\}$ in areas D_α $(\alpha = i, s, e)$ for P-polarization will have the form

$$\mathbf{E}_\alpha^N = \sum_{m=0}^{M}\sum_{n=1}^{N_\alpha^m}\left\{p_{mn}^\alpha \frac{j}{k\varepsilon_\alpha}\nabla\times\nabla\times\mathbf{A}_{mn}^{1,\alpha} + q_{mn}^\alpha \frac{1}{\varepsilon_\alpha}\nabla\times\mathbf{A}_{mn}^{2,\alpha}\right\} + \sum_{n=1}^{N_\alpha^0} r_n^\alpha \frac{j}{k\varepsilon_\alpha}\nabla\times\nabla\times\mathbf{A}_n^{3,\alpha},$$

$$\mathbf{H}_\alpha^N = \frac{j}{k}\nabla\times\mathbf{E}_\alpha^N, \ \alpha = i, s\pm, e. \quad (8)$$

The field inside the shell is represented in the form of „diverging“ $(h_m^{(2)})$ and „arriving“ $(h_m^{(1)})$ waves, i. e.

$$\mathbf{E}_s^N = \mathbf{E}_{s+}^N + \mathbf{E}_{s-}^N, \ \mathbf{H}_s^N = \mathbf{H}_{s+}^N + \mathbf{H}_{s-}^N. \quad (9)$$

It is easy to make sure that the fields (8)–(9) built in this manner satisfy all the conditions of the boundary problem (1)–(4), except for the boundary conditions (2) and (3), set on the interface surfaces with different parameters $\partial D_{i,s}$. Unknown DS amplitudes $\{p_{mn}^{i,s\pm,e}, q_{mn}^{i,s\pm,e}, r_n^{i,s\pm,e}\}$ are determined from these boundary conditions (2) and (3).

Let us briefly discuss the DSM computation scheme. Since the built fields (8) and (9) represent finite sums of the Fourier series in the azimuthal variable φ on the surfaces of revolution $\partial D_{i,s}$, satisfying the boundary conditions on the interfaces reduces to the sequential matching of the Fourier harmonics of the fields on the generatrices of the surfaces of revolution. The DS amplitudes are computed using the generalized collocation method [15] by pointwise matching of the Fourier harmonics of the fields on the generatrix of the surface of revolution. The number of collocation points L remains the same for all m harmonics of the Fourier fields, while the number of DSs may differ for the internal and external fields and may vary depending on the harmonic number m. As a rule, the relation $N_i^m + N_e^m + N_{s+}^m + N_{s-}^m < 4L$ holds, i. e., the corresponding linear systems are overdetermined. The set of DS amplitudes is determined using QR factorization of the corresponding matrices followed by computation of the pseudosolution [16]. Control of the accuracy of the obtained approximate solution can be carried out by calculating the field residual on the surfaces of the layered particle using the found DS amplitudes. The residual is calculated at points intermediate with respect to the collocation points and serves as a reliable criterion for the convergence of the approximated solution to the exact solution of the diffraction problem [11].

In the calculations, we are interested in the energy absorption cross section. For its calculation, we use the optical theorem [17]:

$$\sigma_{\text{abs}} = \sigma_{\text{ext}} - \sigma_{\text{scs}}, \quad (10)$$

here σ_{scs} is the total scattering cross section, σ_{ext} is the extinction cross section, which shows how much energy the scatterer takes from the plane wave for scattering and absorption. The extinction cross section is calculated based on the scattered field pattern [13], whose components in our case take the form

$$F_\theta(\theta, \varphi) = jk_e\sum_{m=0}^{M}(j\sin\theta)^m\cos(m+1)\varphi \times\sum_{n=1}^{N_e^m}\{p_{mn}^e\cos\theta + q_{mn}^e\}\exp\{jk_e z_n^e\cos\theta\} - jk_e\sin\theta\sum_{n=1}^{N_e^0} r_n^e\exp\{jk_e z_n^e\cos\theta\},$$

$$F_\varphi(\theta, \varphi) = -jk_e\sum_{m=0}^{M}(j\sin\theta)^m\sin(m+1)\varphi \times\sum_{n=1}^{N_e^m}\{p_{mn}^e + q_{mn}^e\cos\theta\}\exp\{jk_e z_n^e\cos\theta\}.$$

The extinction cross section, in turn, is determined through the pattern as

$$\sigma_{\text{ext}}(\lambda, \theta_0) = -\frac{4\pi}{k_e}\,\text{Im}F_\theta(\pi - \theta_0, \pi). \quad (11)$$

The scattering cross section is the following:

$$\sigma_{\text{scs}}(\lambda, \theta_0) = \int_0^{2\pi} d\varphi \int_0^{\pi}\{|F_\theta(\theta, \varphi)|^2 + |F_\varphi(\theta, \varphi)|^2\}\sin\theta d\theta.$$

As noted above, control of the result accuracy is carried out by calculating the field residual on the core and shell surfaces, which allows obtaining reliable results for both near and far fields.

Numerical results

Consider a core-shell layered NP. As the basic geometry, we choose a prolate spheroid with an equivolume diameter $D = 11$ nm and an aspect ratio $r = b/a = 4$ (here b is the major axis of the spheroid coinciding with the symmetry axis OZ, a is the minor axis). Let the plasmonic core be surrounded by a dielectric shell of thickness $d = 4$ nm such that the shell surface is a spheroidal surface equidistant from the core at the pole and equator of the spheroidal core. That is, it is a spheroidal surface with axes $a + d$ and $b + d$. In the basic geometry, we assume the spheroid axis sizes to be $b = 28$ nm, $a = 7$ nm. Note that in practice, rods with aspect ratios from 2 to 6 and coating thicknesses from 3 to 30 nm [18]. As the base coating, we choose CTAB (cetyltrimethylammonium bromide) material with refractive index $\sqrt{\varepsilon_s} = 1.526$ [7]. Note that in practice, PEG (polyethylene glycol) material with refractive index $\sqrt{\varepsilon_s} = 1.457$ is also sometimes used. As plasmonic core materials, we consider gold (Au) and silver (Ag). It should be noted that silver is more prone to oxidation, so choosing a reliable protective coating for silver is crucial for ensuring long-term stability during PTT. We assume that the layered particle is located in an absorption-free external medium modeling a female breast, with refractive index $\sqrt{\varepsilon_e} = 1.405$ [19]. Let the P-polarized plane wave propagate in a direction perpendicular to the symmetry axis of the particle ($\theta_0 = 90^\circ$), and the electric field vector lie in the plane XZ and be parallel to the major axis of the spheroid. As will be shown below, this excitation configuration ensures the maximum PR amplitude.

The quantum parameters necessary for computing the Feibelman parameter for gold and silver are taken from [20]:

$$\text{Au}: \quad \hbar\omega_p = 9.02\,\text{eV}, \quad \hbar\gamma = 0.071\,\text{eV},$$

$$v_F = 1.39 \cdot 10^{12}\,\mu\text{m/s}, \quad \mathcal{D} = 8.62 \cdot 10^8\,\mu\text{m}^2/\text{s},$$

$$\text{Ag}: \quad \hbar\omega_p = 9.17\,\text{eV}, \quad \hbar\gamma = 0.021\,\text{eV},$$

$$v_F = 1.39 \cdot 10^{12}\,\mu\text{m/s}, \quad \mathcal{D} = 9.62 \cdot 10^8\,\mu\text{m}^2/\text{s}.$$

Here, ω_p is the plasma frequency of the metal, γ is the Drude damping rate, v_F is the Fermi velocity, $\mathcal{D}$ is the electron diffusion coefficient, $\hbar$ is the reduced Planck constant. Refractive indices of gold and silver with account of frequency dispersion were taken from database [21].

In calculations we use the analytical formula for Feibelman parameter obtained in paper [22], namely

$$d_\perp(\omega) = -j\,\frac{\varepsilon_i\varepsilon_s}{\varepsilon_i - \varepsilon_s}\,\frac{\sqrt{\beta^2 + \mathcal{D}(\gamma + j\omega)}}{\omega_p\sqrt{\varepsilon_b}}\left(\frac{\varepsilon_b}{\varepsilon_i} - 1\right)^{1.5}, \tag{12}$$

where

$$\varepsilon_b = \varepsilon_i + \frac{\omega_p^2}{\omega(\omega - j\gamma)}, \quad \beta^2 = \frac{3}{5}\,v_F^2.$$

It is formula (12) that makes it possible to consider plasmonic metals with different dielectric coating.

Let us move on to discussing the numerical results. Fig. 1 shows the comparative results for the absorption cross section (10) depending on the wavelength λ of external excitation, obtained for Au (Fig. 1, *a*) and Ag (Fig. 1, *b*). In both cases a homogeneous particle without a coating (homogeneous, hmg) is compared to layered particles that have different PEG and CTAB coatings. The classical case (local response approximation, lra) is the curves with markers, accounting for QE using mesoscopic boundary conditions (surface response functions, srf) — solid curves.

Substantial differences are seen in the figure between the curves built for gold and silver. First, the PR amplitude for the silver core is four times larger than the amplitude for the gold core. Second, the maximum for gold lies almost 100 nm to the right of the silver maximum, closer to the right edge of the biological tissue transparency window. Moreover, the curve for silver is much sharper. At the same time, the shift to the short-wavelength area (blue shift) for both metals is approximately the same at 15 nm, and the reduction in PR amplitude (damping) is also nearly identical at about 5 %. Note that in the presence of a coating, the reduction in PR amplitude remains the same as in the case of a homogeneous particle. In addition, increasing the coating density naturally leads to the PR shift to the long-wavelength area (red shift).

As an example, we provide the calculation details for the 4th curve in Fig. 1, *a*, corresponding to the Au@CTAB particle, $D = 11$ nm, $r = 4$, $d = 4$ nm, with mesoscopic boundary conditions (srf). In this case, the relative residual in the l_2 norm was less than 0.4 %, providing for 3 stable digits of the absorption cross section σ_{abs} over the entire wavelength range. This involved 3 Fourier harmonics ($m = 0$, 1 and the φ-independent harmonic), the total number of collocation points on both surfaces was $L = 542$, and the number of sources for field representation was $N_i^m = N_e^m = N_{s-}^m = N_{s+}^m = 68$.

We will further limit ourselves to considering particles with a silver core. Fig. 2, *a* shows the calculation results for the absorption cross section of particles with basic geometry and different degrees of prolation. It can be seen that increasing the aspect ratio ($r = 3.5$, 4, 4.5) of the spheroid pushes the PR deeper into the transparency window of biological tissues. The influence of QEs is reduced to a blue shift of the PR. Fig. 2, *b* shows the results corresponding to variation of the equivolume diameter of the silver core ($D = 11$, 12, 13 nm). It is interesting to note that the position of the PR absorption cross section in the wavelength area is practically independent of the diameter variation within these limits.

Fig. 3, *a* shows graphs of the scattering cross section for variations in the thickness of the CTAB dielectric coating

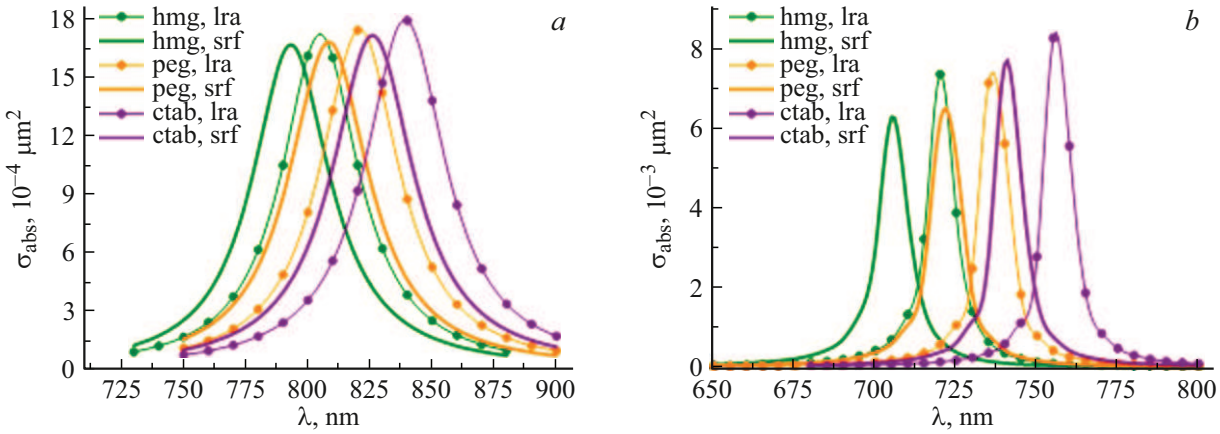

Figure 1. Comparison of local (lra) and mesoscopic (srf) approaches for gold (*a*) and silver (*b*) particles without a coating (hmg) and with PEG and CTAB coatings. PR amplitude in case of Ag is 4 times more than in Au.

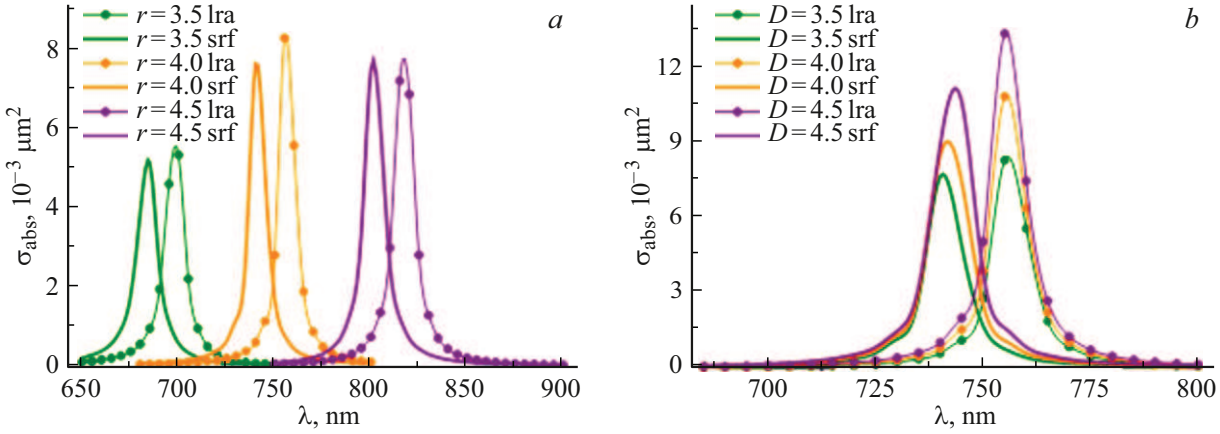

Figure 2. Dependence of absorption cross section of a silver particle with a CTAB coating on core prolateness (*a*) and equivolume diameter of the core (*b*): comparison of the results obtained using a local (lra) and mesoscopic (srf) approaches. Increase in prolateness causes PR shift towards the long wavelength region. Poor variation of the core size somewhat affects the PR amplitude, but its position will not change.

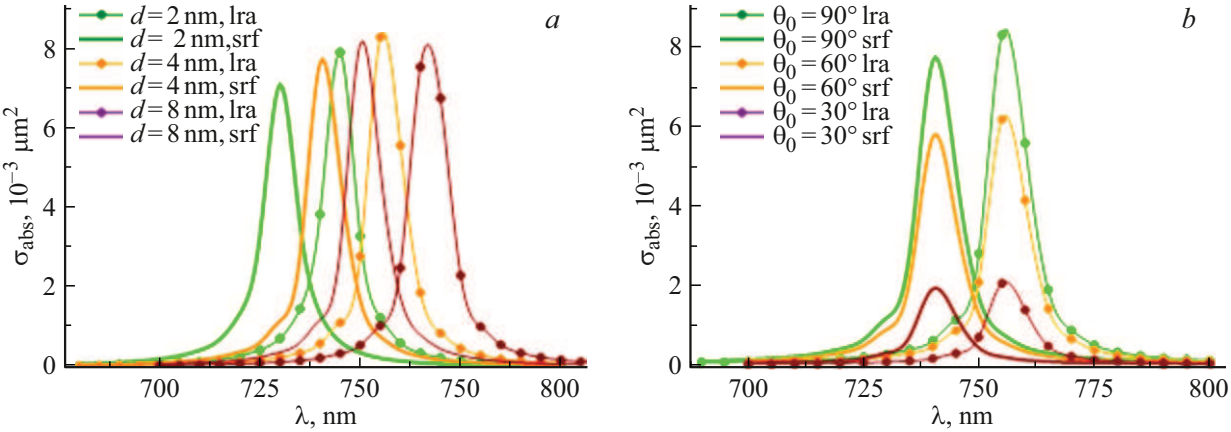

Figure 3. Dependence of absorption cross section of a silver particle with a CTAB coating on coating thickness (*a*) and angle of incidence of a plane wave (*b*): comparison of the results obtained using a local (lra) and mesoscopic (srf) approaches. Increasing coating thickness shifts the PR to the long-wavelength region, apparently due to the increase in particle size. With oblique incidence, the z-components of the field decreases and the PR amplitude significantly drops.

($d = 2, 4, 8$ nm). The red shift apparently occurs due to the increase in the overall size of the layered particle, while the influence of QEs reduces to a blue shift of 15 nm. Fig. 3, *b* is devoted to the study of the absorption cross section of a layered particle of basic configuration with varying plane wave incidence angle ($\theta_0 = 30°, 60°, 90°$). It is clearly seen that as the incidence angle decreases, the PR amplitude also decreases. At the same time, the blue shift arising from accounting for QEs remains constant at 15 nm.

Conclusion

Let us formulate the main results obtained in this paper.

1. The discrete sources method has been successfully adapted to study the manifestation of QEs in the plasmonic core of a layered NP. The QEs were taken into account based on mesoscopic boundary conditions with Feibelman parameters.

2. A comparative analysis of the absorption cross section of layered particles with nanoscale gold and silver cores was carried out. As a result, it was found that the dielectric coating does not affect the photothermal properties of layered NPs. At the same time, the particles with silver cores exhibit four times higher absorbed energy values than gold ones. Accounting for QEs leads to the blue shift of the PR position by 15 nm with a slight decrease in its amplitudes by about 5 %.

3. It was shown that varying the core prolation at a constant coating thickness allows shifting the absorption cross section maximum deeper into the transparency region of biological tissues. Poor variation of the equivolume core diameter practically does not change the PR position in the wavelength range.

4. It was found that changing the plane wave incidence angle with respect to the particle symmetry axis significantly reduces the absorption cross section value, while leaving the shift between the classical and mesoscopic PR constant at 15 nm.

Funding

The authors' studies were supported by the Moscow Center for Fundamental and Applied Mathematics at Lomonosov Moscow State University under agreement № 075-15-2025-345.

Conflict of interest

The authors declare that they have no conflict of interest.

References

[1] L. Liz-Marzán. Ed. *Colloidal Synthesis of Plasmonic Nanometals* (Jenny Stanford Publishing, N.Y., 2021).

[2] A. Andleeb, A. Andleeb, S. Asghar, G. Zaman, M. Tariq, A. Mehmood, M. Nadeem, C. Hano, J.M. Lorenzo, B.H. Abbasi. Cancers (Basel), **13** (11), 2818 (2021). DOI: 10.3390/cancers13112818

[3] W.H. Skinner, M. Salimi, L. Moran, I. Blein-Dezayes, M. Mehta, S. Mosca, A.-G. Vaideanu, B. Gardner, F. Palombo, A.G. Schätzlein, P. Matousek, T. Harries, N. Stone. J. Phys. Chem. C, **129** (3), 1864 (2025). DOI: 10.1021/acs.jpcc.4c06381

[4] N. Hlapisi, S.P. Songca, P.A. Ajibade. Pharmaceutics, **16** (10), 1268 (2024). DOI: 10.3390/pharmaceutics16101268

[5] H.S. Han, K.Y. Choi. Biomedicines, **9** (3), 305 (2021). DOI: 10.3390/biomedicines9030305

[6] O. Gherasim, R.A. Puiu, A.C. Bîrcă, A.-C. Burduşel, A.M. Grumezescu. Nanomaterials, **10** (11), 2318 (2020). DOI: 10.3390/nano10112318

[7] P. Singh, S. Pandit, S.R. Balusamy, M. Madhusudanan, H. Singh, H.M. Amsath Haseef, I. Mijakovic. Advanced Healthcare Materials, **14** (4), e2403059 (2024). DOI: 10.1002/adhm.202403059

[8] W.A. Arcos Rosero, A. Bueno Barbezan, C. Daruich de Souza, M.E. Chuery Martins Rostelato. Pharmaceutics, **16** (2), 255 (2024). DOI: 10.3390/pharmaceutics16020255

[9] C. Tserkezis, W. Yan, W. Hsieh, G. Sun, J.B. Khurgin, M. Wubs, N.A. Mortensen. Int. J. Mod. Phys. B, **31** (24), 1740005 (2017). DOI: 10.1142/S0217979217400057

[10] P.E. Stamatopoulou, C. Tserkezis. Opt. Materials Express, **12** (5), 1869 (2022). DOI: 10.1364/OME.456407

[11] Yu.A. Eremin, A.G. Sveshnikov. Computat. Math. Math. Phys., **61** (4), 564 (2021). DOI: 10.1134/S0965542521040047

[12] N.A. Mortensen. Nanophotonics, **10** (10), 2563 (2021). DOI: 10.1515/nanoph-2021-0156

[13] Yu.A. Eremin, V.V. Lopushenko. Opt. i spektr., **133** (7), 783 (2025) (in Russian). DOI: 10.61011/OS.2025.07.61113.8146-25

[14] D. Colton, R. Kress. *Integral Equation Methods in Scattering Theory* (John Wiley & Son, N.Y., 1983).

[15] N.S. Bakhvalov. *Numerical methods* (MIR Publishers, M., 1977).

[16] V.V. Voevodin, Yu.A. Kuznetsov. *Matritsy i vychisleniya* (Nauka, M., 1984) (in Russian).

[17] Kh. Khenl, A. Maue, K. Vestpfal. *Teoriya difraktsii* (Mir, M., 1964) (in Russian).

[18] N.G. Khlebtsov, S.V. Zarkov. J. Phys. Chem. C, **128** (36), 15029 (2024). DOI: 10.1021/acs.jpcc.4c03126

[19] Y. Eremin, V. Lopushenko. Nanomaterials, **11** (12), 3297 (2021). DOI: 10.3390/nano11123297

[20] S. Raza, S.I. Bozhevolnyi, M. Wubs, N.A. Mortensen. J. Physics: Condensed Matter, **27** (18), 183204 (2015). DOI: 10.1088/0953-8984/27/18/183204

[21] M.N. Polyanskiy. Refractiveindex.info Database of Optical Constants, Scientific Data, **11** (1), 94 (2024). DOI: 10.1038/s41597-023-02898-2

[22] M.H. Eriksen, C. Tserkezis, N.A. Mortensen, J.D. Cox. Nanophotonics, **13** (15), 2751 (2024). DOI: 10.1515/nanoph-2023-0575

Translated by M.Verenikina